NEUROSCIENCE

Disruption of BAG3-mediated BACE1 stabilization alleviates neuropathology and memory deficits in a mouse model of Alzheimer's disease

Lei Xia[1], Junjie Li[1], Yayan Pang[1], Chunfang Dai[1,2], Mingliang Xu[1], Yehong Du[1], Qiuyun Tian[1], Lilin Yi[1], Bin Wu[1], Mulan Chen[1], Yiqiong Qiu[3], Chongjie Cheng[4], Yu Tian Wang[5], Weihong Song[6,7], Zhifang Dong[1]*

β-Site amyloid precursor protein (APP)–cleaving enzyme 1 (BACE1) is the rate-limiting enzyme for amyloid-β (Aβ) generation and is considered promising drug target for Alzheimer's disease (AD). The co-chaperone BAG3 (Bcl-2–associated athanogene 3) plays an important role in maintaining intracellular protein homeostasis by regulating heat shock protein 70 (HSP70). Here, we reported that BAG3 expression was significantly elevated in AD. It interacted with and stabilized BACE1 by delaying its degradation through ubiquitin-proteasome and autophagy-lysosomal pathways. BAG3^{E455K} and BAG3^{R480A} mutations reduced their interaction with BACE1. SPOT peptide arrays revealed that BACE1 carboxyl-terminal peptide fragments bound to the RQ domain of BAG3. This interaction can be disrupted by BACE1-derived peptide (Tat-BACE1$_{480-494}$), leading to decreased BACE1 stability. In APP23/PS45 double transgenic mice, Tat-BACE1$_{480-494}$ reduced BACE1 levels, decreased Aβ production, and improved synaptic and cognitive deficits. These findings indicate that BAG3 forms complex with HSP70 and BACE1 to stabilize BACE1, suggesting that Tat-BACE1$_{480-494}$, may represent an ideal class of neuroprotective therapeutics against AD.

INTRODUCTION

Alzheimer's disease (AD) is one of the most common neurodegenerative disorders causing progressive dementia. Its pathological hallmarks include extracellular amyloid plaque depositions, intracellular tau neurofibrillary tangles, and synaptic abnormalities (*1*). Under physiological conditions, amyloid precursor protein (APP) is mainly cleaved by a disintegrin and metalloproteinase 10 (ADAM10) and γ-secretase in a non-amyloidogenic pathway (*2*). In AD, APP is mainly cleaved by the β-site of APP-cleaving enzyme 1 (BACE1) and γ-secretase to produce amyloid-β (Aβ) peptides. During this amyloidogenic process, BACE1 serves as the initial and rate-limiting enzyme in Aβ generation (*3*). Therefore, inhibiting BACE1 has emerged as a potential therapeutic strategy for AD. However, genetic deletion of BACE1 is not an ideal choice due to its physiological role in regulating energy metabolism and synaptic homeostasis through cleavage of various substrates (*4*). Despite numerous clinical trials, nearly all BACE1 inhibitors have failed in later phases due to efficacy or safety concerns (*5*–*7*), underscoring the ongoing need for safe and effective therapies targeting BACE1 in AD.

Bcl-2–associated athanogene 3 (BAG3) is a 575–amino acid protein that is widely expressed, with prominent expression in the brain, cardiac muscle, skeletal muscle, and many cancers (*8*–*10*). BAG3 modulates diverse biological processes such as apoptosis, development, cytoskeleton organization, and autophagy, through its multiple protein-protein binding domains (*11*–*15*). As a scaffold protein, BAG3 binds to heat shock protein 70 (HSP70) via its BAG domain and to heat shock protein beta 8 (HSPB8) through two Ile-Pro-Val (IPV) motifs, forming a HSP70-BAG3-HSPB8 ternary complex. This complex inhibits the ubiquitin-proteasome degradation but promotes autophagy-lysosomal degradation (*16*–*18*). It has been reported that BAG3-mediated selective macroautophagy is crucial for the clearance of aggregated proteins associated with AD and other neurodegenerative disorders (*16*, *17*, *19*, *20*). However, accumulating evidence has shown that the expression of BAG3 is significantly elevated (*21*–*25*), but AD-related pathological proteins such as APP, Tau, and BACE1 are markedly increased because of impaired autophagy function in AD (*26*–*28*). One possible reason is that BAG3 not only mediates protein degradation through autophagy but also acts as a nucleotide exchange factor to promote the aggregation of ubiquitinated proteins by directly binding and inhibiting the HSP70-mediated ubiquitin-proteasome system, thereby increasing protein stability (*29*). For example, BAG3 can stabilize HSPB8 by forming a BAG3-HSP70-HSPB8 ternary complex and reduce the apoptosis of cardiomyocytes induced by hypoxia (*29*, *30*). BAG3 can also stabilize signal transducer and activator of transcription 3 and the anti-apoptotic protein myeloid cell leukemia–1 (Mcl-1) to enhance the anti-apoptotic effect of tumor cells (*31*, *32*). Furthermore, BAG3 can directly bind to glutaminase (GLS) and occupies its ubiquitination site, thereby stabilizing GLS in the form of BAG3-GLS binary complex (*33*). Meanwhile, a recent report has shown that oxygen-regulated protein 150, as a chaperone, interacts with and stabilizes BACE1 at posttranslational level, while its down-regulation reverses this chaperone function, leading to BACE1 degradation (*34*). Therefore, given its high expression, co-chaperone BAG3 may similarly stabilize BACE1.

In this study, we detected the expression of BAG3 and its interaction with BACE1 to determine its effect on the stability of BACE1 in

[1]Growth, Development, and Mental Health of Children and Adolescence Center, Pediatric Research Institute, Ministry of Education Key Laboratory of Child Development and Disorders, National Clinical Research Center for Child Health and Disorders, Chongqing Key Laboratory of Child Neurodevelopment and Cognitive Disorders, Children's Hospital of Chongqing Medical University, Chongqing 400014, China. [2]Department of Children Health Care, Guangzhou Women and Children's Medical Center, Guangzhou Medical University, Guangzhou, Guangdong 510623, China. [3]Clinical Laboratory of Changshou District Hospital of Traditional Chinese Medicine, Chongqing 401220, China. [4]Department of Neurosurgery, The First Affiliated Hospital of Chongqing Medical University, Chongqing 400016, China. [5]Department of Medicine, Brain Research Centre, Vancouver Coastal Health Research Institute, University of British Columbia, Vancouver, BC V6T 2B5, Canada. [6]Center for Geriatric Medicine, Key Laboratory of Alzheimer's Disease of Zhejiang Province, The First Affiliated Hospital and Institute of Aging, Wenzhou Medical University, Wenzhou, Zhejiang 325000, China. [7]Oujiang Laboratory (Zhejiang Lab for Regenerative Medicine, Vision and Brain Health), Wenzhou, Zhejiang 325001, China.
*Corresponding author. Email: zfdong@cqmu.edu.cn

AD. Furthermore, we developed an interfering peptide derived from endogenous BACE1 to disrupt the interaction between BAG3 and BACE1 and investigated whether it could promote BACE1 degradation and ameliorate AD-related pathology and memory decline in AD model mice.

RESULTS

Expressions of BAG3 and BACE1 are increased in AD

To investigate the role of BAG3 in AD, we introduced APP23/PS45 double transgenic mice in our study. The results showed that the expressions of APP (Fig. 1, A and B), presenilin 1 (PS1) (Fig. 1, A and C), BACE1 (Fig. 1, A and D), and APP carboxyl terminal hydrolytic fragment β (CTF-β) (Fig. 1, A and E) were significantly increased in the hippocampus of 3-month-old AD model mice compared to that of age-matched wild-type (WT) mice. According to Gene Expression Omnibus (GEO) analysis, BAG3 is highly expressed in the hippocampus of patients with AD and aging mice, but not in peripheral blood of patients (fig. S1, A to F). Similarly, we observed a significant elevation in the expression of BAG3 in the hippocampus of AD model mice compared to that of WT controls (Fig. 1, A and I). Given that BAG3 plays a crucial role in macroautophagy regulation through forming a BAG3-HSP70-HSPB8 ternary complex, we further examined the expression of HSP70, HSPB8 and autophagy-related proteins. The results showed that HSP70 remained unchanged (Fig. 1, A and J), whereas HSPB8 (Fig. 1, A and F) was significantly decreased in the hippocampus of AD model mice compared to that of WT mice. Furthermore, autophagy-related protein P62 markedly elevated, while the ratio of microtubule-associated protein1 light chain 3-II (LC3-II) to LC3-I (LC3-II/I) significantly decreased in the hippocampus of AD model mice compared to that of WT mice (Fig. 1, G and H), suggesting impaired autophagy function in AD.

Consistent with our findings in AD model mice, the expressions of APP, BACE1, and BAG3 were significantly increased, whereas HSPB8 was reduced in $N2A^{APP}$ (Fig. 1, K to N; Fig. 1P) and 20E2 and 2EB2 cells (Fig. 1, S to V; Fig. 1X) compared to that in N2A and human embryonic kidney (HEK) 293 cells, respectively. HSP70 expression was markedly decreased in $N2A^{APP}$ cells (Fig. 1O), but it was significantly increased in 20E2 and 2EB2 cells (Fig. 1W). Together, these results suggest that BAG3 expression is significantly elevated in AD, but its role in mediating macroautophagy appears to be compromised, as evidenced by reduced HSPB8 levels and impaired autophagy function.

BAG3 increases the stability of BACE1

Next, we wanted to determine the effects of BAG3 on BACE1 expression. The results showed that overexpression of BAG3 increased the levels of BACE1 in HEK293 (Fig. 2, A to C) and 20E2 cells (Fig. 2, G to I), respectively. In contrast, down-regulation of BAG3 decreased BACE1 in HEK293 (Fig. 2, A to C) and 20E2 cells (Fig. 2, G to I). To examine the effect of BACE1 on BAG3 expression, HEK293B2 (HEK293 cells stably expressing BACE1) was introduced (fig. S2, A and B). The results showed that BAG3 was significantly reduced in HEK293B2 compared to that in HEK293 cells (fig. S2, A and C). Given the elevated levels of BAG3 and P62 and the decreased levels of LC3-II/I observed in AD model mice, we next examined the effects of BAG3 on LC3-II/I and P62 in HEK293 and 20E2 cells. We found that overexpression of BAG3 increased LC3-II/I, whereas its knockdown decreased LC3-II/I in HEK293 (Fig. 2, A and F) and 20E2 cells (Fig. 2, G and L). However, unlike the increased expression of P62 in the hippocampus of AD mice (Fig. 1, A and G), it was decreased or unchanged in HEK293 (Fig. 2, A and E) and 20E2 cells (Fig. 2, G and K) overexpressing BAG3, respectively. Notably, HSPB8 was significantly decreased in 20E2 cells (Fig. 2, G and J) overexpressing BAG3, but not in HEK293 cells (Fig. 2, A and D). In addition, HSPB8 was also significantly decreased in HEK293B2 cells (fig. S2, A and D), indicating that overexpression of BACE1 alone reduces HSPB8 expression.

It has been reported that BACE1 can undergo degradation through the ubiquitin-proteasome and autophagy-lysosomal pathways (*35*, *36*). Consistently, we found that the proteasome inhibitor MG132 and autophagy inhibitor chloroquine (CQ) effectively blocked BACE1 degradation in HEK293 cells (Fig. 2, M and O). BAG3 overexpression enhanced the inhibitory effects of MG132 and CQ on BACE1 degradation (Fig. 2, M to O). BAG3 knockdown significantly reduced BACE1 levels, an effect that could be partially reversed by the proteasome inhibitor MG132, but not by the autophagy inhibitor CQ (Fig. 2, P and R). Co-immunoprecipitation results further demonstrated that BAG3 knockdown promoted BACE1 polyubiquitination, while BAG3 overexpression inhibited it (fig. S12). Moreover, cycloheximide (CHX) was chosen to inhibit protein synthesis, revealing that endogenous BACE1 protein levels significantly decreased after 48 hours of CHX exposure, while BAG3 overexpression delayed this process in HEK293 cells (Fig. 2, S to U). Together, these results indicate that BAG3 increases BACE1 level by inhibiting the ubiquitin-proteasome and autophagy-lysosomal pathways.

BAG3 stabilizes BACE1 by forming HSP70-BAG3-BACE1 complex

In addition to its role in mediating macroautophagy, BAG3 can also bind to HSP70 and inhibit its mediated ubiquitination proteasome pathway (*37*). Therefore, we next wanted to determine whether BAG3 interacts with BACE1 to stabilize it. We first examined the interaction between BAG3 and BACE1 and found that BAG3 could interact with BACE1 (Fig. 3, A to C). In addition, we also found that the interaction between BAG3 and BACE1 was markedly increased in AD model cells including $N2A^{APP}$ and 20E2 and 2EB2, compared to their respective controls, N2A and HEK293 cells (Fig. 3, A and B). Knockdown of BAG3 decreased its interaction with BACE1, whereas overexpression of BAG3 increased their interactions in HEK293 cells (Fig. 3C).

Although BAG3 can stabilize proteins like GLS by forming a "BAG3-GLS" binary complex (*33*), it commonly stabilizes other proteins through complexes like "HSP70-BAG3-X," such as HSP70-BAG3-HSPB8 and HSP70–BAG3–Mcl-1 (*29*, *30*, *32*). In addition, BAG3 binds to HSP70 through its BAG domain, and mutations such as E455K in this region can disrupt the HSP70-BAG3 interaction, affecting the stability of the HSP70-BAG3-X complex. Considering the ability of BAG3 to interact with and increase BACE1 levels, it is reasonable to speculate that BAG3 may have a critical role in mediating BACE1 stabilization in AD. To determine whether BAG3 stabilizes BACE1 through forming BAG3-BACE1 or HSP70-BAG3-BACE1 complex, we analyzed the three-dimensional configuration of the BAG domain and reported point mutations (Fig. 3, D and E). We constructed plasmids (Flag-$BAG3^{E455K}$ and Flag-$BAG3^{R480A}$) with point mutation in the BAG domain to assess whether these mutations can block the interaction between HSP70 and BAG3. The results indicated that mutations E455K and R480A, located in the α2 and α3

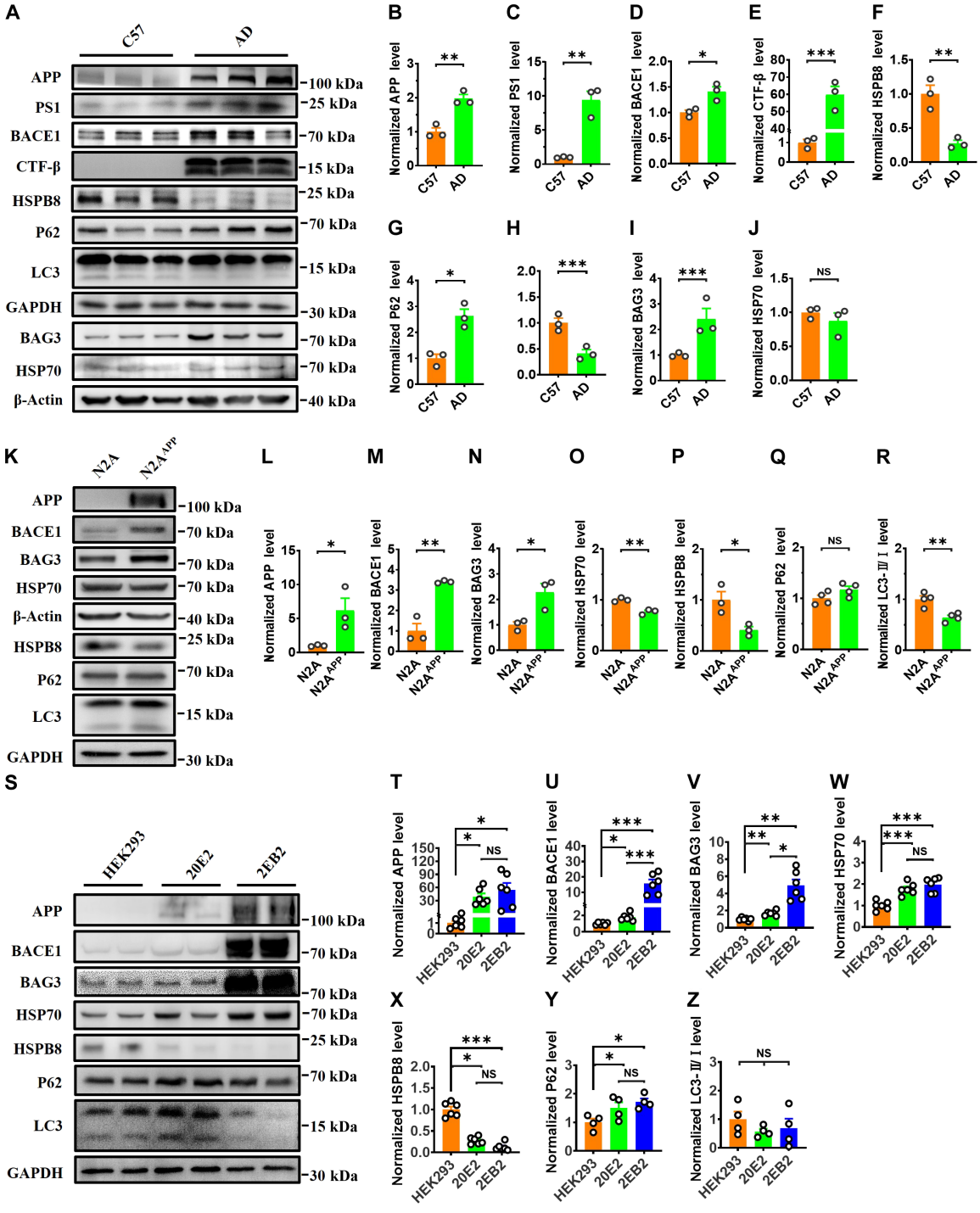

Fig. 1. Expression of BAG3 is increased in AD model mice and cells. (**A** to **J**) Protein levels of APP, PS1, BACE1, CTF-β, HSPB8, P62, LC3-II/I, BAG3, and HSP70 in the hippocampus of APP23/PS45 double transgenic aged 3 months ($n = 3$ in each group). (**K** to **R**) Protein levels of APP, BACE1, BAG3, HSP70, HSPB8, P62, and LC3-II/I in N2A and $N2A^{APP}$ cells ($n = 3$ in each group). (**S** to **Z**) Protein levels of APP, BACE1, BAG3, HSP70, HSPB8, P62, and LC3-II/I in HEK293, 20E2, and 2EB2 cells ($n = 3$ in each group). All data are expressed as means ± SEM. $^{*}P < 0.05$; $^{**}P < 0.01$; $^{***}P < 0.001$; not significant (NS). Statistical analyses were performed using a two-tailed unpaired Student's *t* test (B to J and L to R) or one-way analysis of variance (ANOVA) followed by least significant difference (LSD) multiple comparisons test for homogeneous variance or Dunnett's multiple comparisons test for heterogeneous variance (T to Z). GAPDH, glyceraldehyde-3-phosphate dehydrogenase.

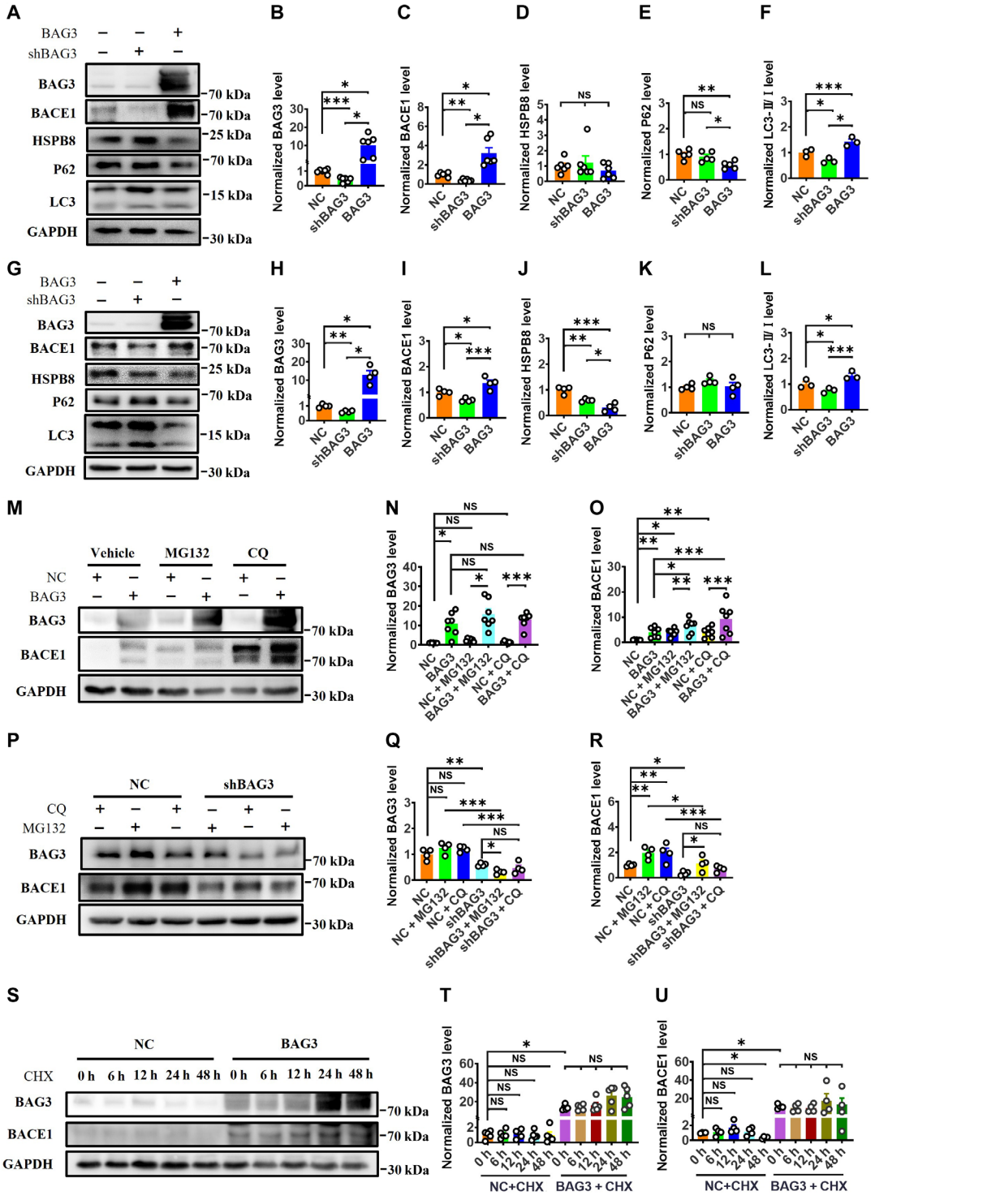

Fig. 2. Overexpression of BAG3 increases BACE1 levels. (**A** to **F**) Protein levels of BAG3, BACE1, HSPB8, P62, and LC3-II/I in HEK293 after BAG3 overexpression or knockdown ($n = 3$ to 6 in each group). (**G** to **L**) Protein levels of BAG3, BACE1, HSPB8, P62, and LC3-II/I in 20E2 after BAG3 overexpression or knockdown ($n = 3$ to 4 in each group). (**M** to **O**) The effect of MG132 or CQ treatment on BAG3 and BACE1 expression in HEK293 cells overexpressing BAG3 ($n = 7$ in each group). (**P** to **R**) The effect of MG132 or CQ treatment on BAG3 and BACE1 expression in HEK293 cells with BAG3 knockdown ($n = 4$ in each group). (**S** to **U**) The effect of CHX treatment on BAG3 and BACE1 expression in HEK293 cells overexpressing BAG3 ($n = 4$ in each group). All data are expressed as means ± SEM. $^*P < 0.05$; $^{**}P < 0.01$; $^{***}P < 0.001$; not significant (NS). Statistical analyses were performed using one-way ANOVA followed by LSD multiple comparisons test for homogeneous variance or Dunnett's multiple comparisons test for heterogeneous variance.

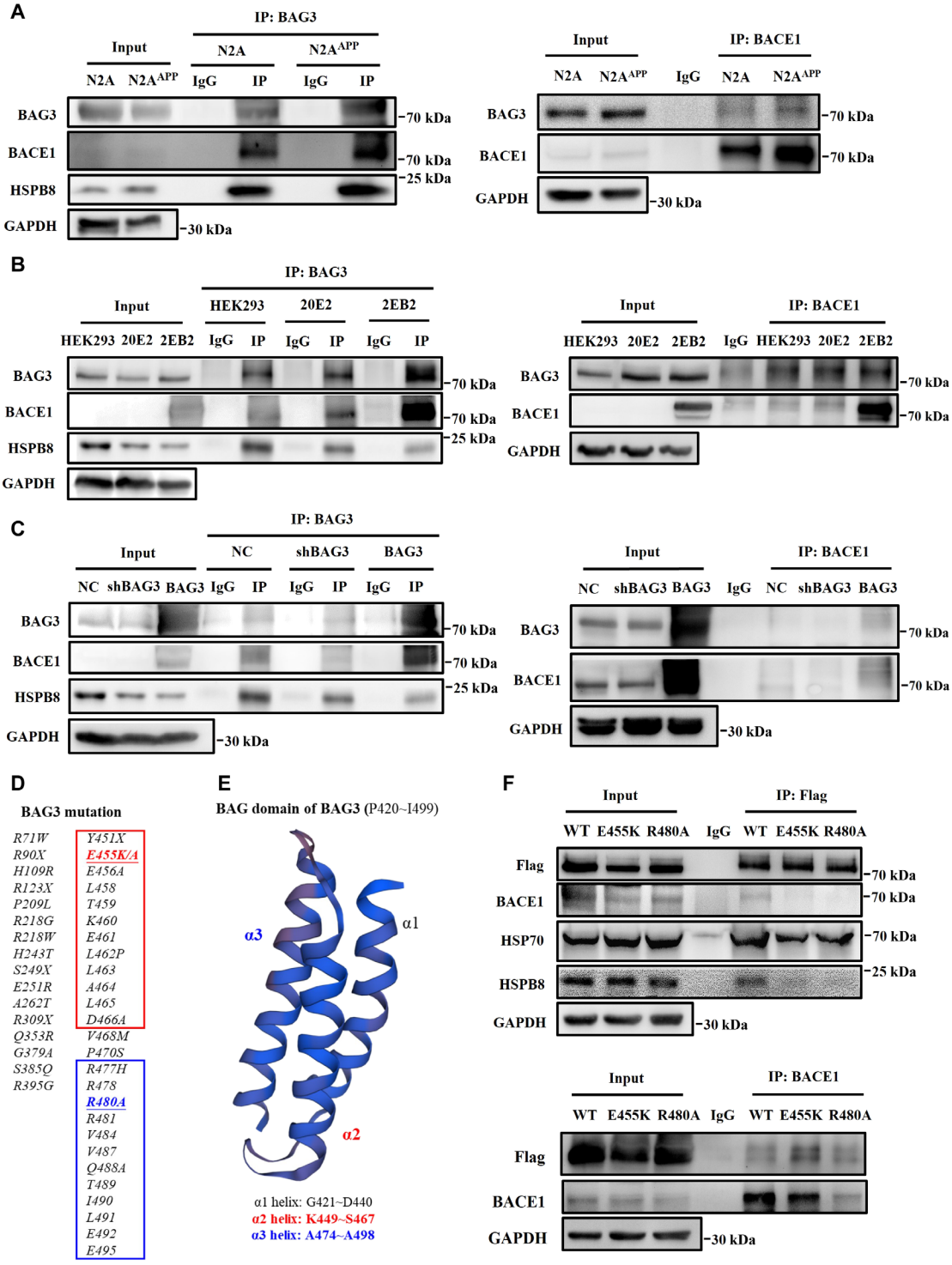

Fig. 3. BAG3 stabilizes BACE1 by forming HSP70-BAG3-BACE1 complex. (**A** and **B**) The interaction between BAG3 and BACE1 in N2A, N2A^{APP}, HEK293, 20E2, and 2EB2 cells. (**C**) The interaction between BAG3 and BACE1 in HEK293 cells overexpressing or knocking down BAG3. IP, immunoprecipitation. (**D**) The main mutation sites of BAG3. (**E**) Three-dimensional structure of the BAG domain in BAG3. (**F**) The interaction between BAG3 and BACE1, HSP70, and HSPB8 in HEK293 cells transfecting Flag-BAG3^{WT}, Flag-BAG3^{E455K}, or Flag-BAG3^{R480A} plasmid.

helices of the BAG domain of BAG3, reduced interactions between HSP70 and BAG3, as well as between BAG3 and BACE1 (Fig. 3F). Combined with the earlier findings that reduced interaction between BAG3 and BACE1 correlates with decreased BACE1 levels (Fig. 3C), it suggests that BAG3 stabilizes BACE1 by forming an HSP70-BAG3-BACE1 complex.

Furthermore, to explore the direct interaction site between BAG3 and BACE1, we conducted peptide array analysis and identified the previously unknown E101-H112 region of human BAG3 as capable of directly binding purified human BACE1 protein (fig. S3, A and B). Given that BAG3 proteins in various species generally contain RQ sequences in this region (table S1), we termed this region (E101-H112 region) the "RQ domain" of the BAG3 protein. This RQ domain is adjacent to and overlaps with an amino acid sequence of a known IPV motif (P87-E101) that directly binds HSPB8 (fig. S3, A and B), suggesting a potential competition between BACE1 and HSPB8 for BAG3 binding. While the interaction between BAG3 and BACE1 was enhanced, the interaction between BAG3 and HSPB8 was notably reduced in HEK293 cells overexpressing BAG3 (Fig. 3C). Therefore, BACE1 may disrupt the stability of the HSP70-BAG3-HSPB8 complex, thereby inhibiting BAG3-mediated macroautophagy.

To further validate the interaction between BAG3 and BACE1, we used synthetic human BACE1 peptide arrays to bind purified human BAG3 protein. The results showed that I465-A494 region of human BACE1 can directly bind to purified human BAG3 protein (fig. S4, A and B). Molecular docking simulations of BAG3 and BACE1 further supported this interaction, revealing a favorable binding pose and low binding free energy of −1915.42 kcal/mol (fig. S5E). In addition, it has been reported that BACE1 directly binds to reticulon-3 (RTN3), leading to a decrease in BACE1 stability (*38*, *39*). The region where BACE1 binds to BAG3 overlaps with the region where it bound to RTN3 (fig. S4, A and B), indicating that BAG3 may compete with RTN3 for the binding site of BACE1. Given that RTN3 is reduced (*40*) and that BAG3 is increased in the brains of patients with AD, BAG3 may have an advantage in competition with RTN3 for the BACE1 binding site, thereby further contributing to BACE1 stabilization through an alternate mechanism.

Tat-BACE1$_{480\text{-}494}$ peptide alleviates memory deficits in AD model mice

On the basis of the identified binding sites of BACE1 and BAG3, we developed three interfering peptides Tat-BACE1$_{465\text{-}494}$, Tat-BACE1$_{465\text{-}479}$, and Tat-BACE1$_{480\text{-}494}$ (table 2). The peptides were rendered membrane permeable by fusing the cell-membrane transduction domain of the HIV-1 Tat protein. The results showed that Tat-BACE1$_{465\text{-}494}$ was able to significantly reduce BACE1 at 40 μM concentration, without affecting BAG3 levels (fig. S7, A to C) compared to its scrambled peptide sTat-BACE1$_{465\text{-}494}$ (table S2). Unfortunately, Tat-BACE1$_{465\text{-}479}$ was found to be insoluble in cell culture medium due to its sequence containing at least 10 nonpolar hydrophobic amino acids (table S2). Notably, Tat-BACE1$_{480\text{-}494}$, at a concentration of 40 μM, significantly reduced BACE1 levels in both N2A^{APP} and 20E2 cells (fig. S7, E and H) but did not affect APP (fig. S7, F and I) compared to its scrambled peptide sTat-BACE1$_{480\text{-}494}$. Therefore, we next focused on investigating the effect of Tat-BACE1$_{480\text{-}494}$ on the interaction between BACE1 and BAG3. According to the principle of competitive inhibition, Tat-BACE1$_{480\text{-}494}$ was expected to bind with BAG3 and competitively inhibit the interaction between BACE1 and BAG3. Molecular docking simulations indicated that both Tat-BACE1$_{480\text{-}494}$ and BACE1$_{465\text{-}494}$ bound to the RQ domain of BAG3 with low binding free energy (fig. S5, F and G). On the other hand, treatment with Tat-BACE1$_{480\text{-}494}$ at 40 μM reduced the interaction between BAG3 and BACE1 in 20E2 and N2A^{APP} cells (fig. S8, A and B), while the interaction between BAG3 and HSPB8 remained unaffected (fig. S8, A and B). These results suggest that Tat-BACE1$_{480\text{-}494}$ specifically disrupts the BAG3-BACE1 interaction without affecting other interactions involving BAG3.

Given that Tat-BACE1$_{480\text{-}494}$ competitively inhibits the binding of BACE1 to BAG3, we next wanted to assess its therapeutic potential in AD. Two-month-old APP23/PS45 mice were treated with Tat-BACE1$_{480\text{-}494}$ [10 mg/kg per day, intraperitoneally (ip)] or its scramble sTat-BACE1$_{480\text{-}494}$ for 3 months, followed by evaluation of spatial learning and memory (fig. S6). The results showed that daily treatment with Tat-BACE1$_{480\text{-}494}$ did not affect the growth rate and spontaneous locomotion of AD model mice (fig. S10G; Fig. 4, A and B). However, the recognition index (RI) was significantly increased in AD model mice treated with Tat-BACE1$_{480\text{-}494}$ (Fig. 4, C and D), indicating enhanced short-term memory. To further evaluate the effect of Tat-BACE1$_{480\text{-}494}$ on long-term spatial learning and memory, the Morris water maze and Barnes maze tests were conducted. In the Morris water maze test, AD model mice treated with Tat-BACE1$_{480\text{-}494}$ showed significantly shorter escape latency to find the hidden platform during spatial learning period (Fig. 4E), indicating improved spatial learning function. Furthermore, Tat-BACE1$_{480\text{-}494}$ treatment also markedly reduced the latency to first entry into platform zone (Fig. 4F) and increased the entries into the platform zone (Fig. 4G) during the spatial memory probe test in AD model mice, indicating improved spatial memory retrieval. Similar results were observed in the Barnes maze test. AD model mice treated with Tat-BACE1$_{480\text{-}494}$ showed significantly shorter latency to find the escape box (Fig. 4H), indicating improved spatial learning function. During the spatial memory probe test, Tat-BACE1$_{480\text{-}494}$ treatment also markedly shortened the latency to find the escape box (Fig. 4I) and increased the number to find the escape box (Fig. 4J) in AD model mice, indicating improved spatial memory retrieval.

Given that synaptic plasticity, particularly hippocampal CA1 long-term potentiation (LTP), is considered as a cellular mechanism underlying spatial learning and memory, we next examined the effect of Tat-BACE1$_{480\text{-}494}$ on hippocampal CA1 LTP. The results showed that LTP in the hippocampal CA1 region was significantly decreased in AD model mice compared with that in WT mice (Fig. 4, K and L). Tat-BACE1$_{480\text{-}494}$ restored the hippocampal CA1 LTP to control levels in AD model mice (Fig. 4, K and L). Together, these results indicate that treatment with Tat-BACE1$_{480\text{-}494}$ alleviates the impairments of hippocampal CA1 LTP and spatial learning and memory in AD model mice.

Tat-BACE1$_{480\text{-}494}$ peptide alleviates Aβ pathology in AD model mice

To correlate behavioral changes with AD-related neuropathology, we performed biochemical assays on brain tissues immediately after the behavioral tests in these animals. The results showed that Tat-BACE1$_{480\text{-}494}$ significantly reduced the levels of $A\beta_{40}$ in the hippocampus and cortex of AD model mice (Fig. 5, A and B). Although the level of $A\beta_{42}$ remained unchanged in the hippocampus (Fig. 5B), it markedly reduced in the cortex of AD model mice treated with Tat-BACE1$_{480\text{-}494}$ (fig. S9B). Furthermore, treatment with Tat-BACE1$_{480\text{-}494}$ significantly reduced neuritic plaque formation in AD model mice

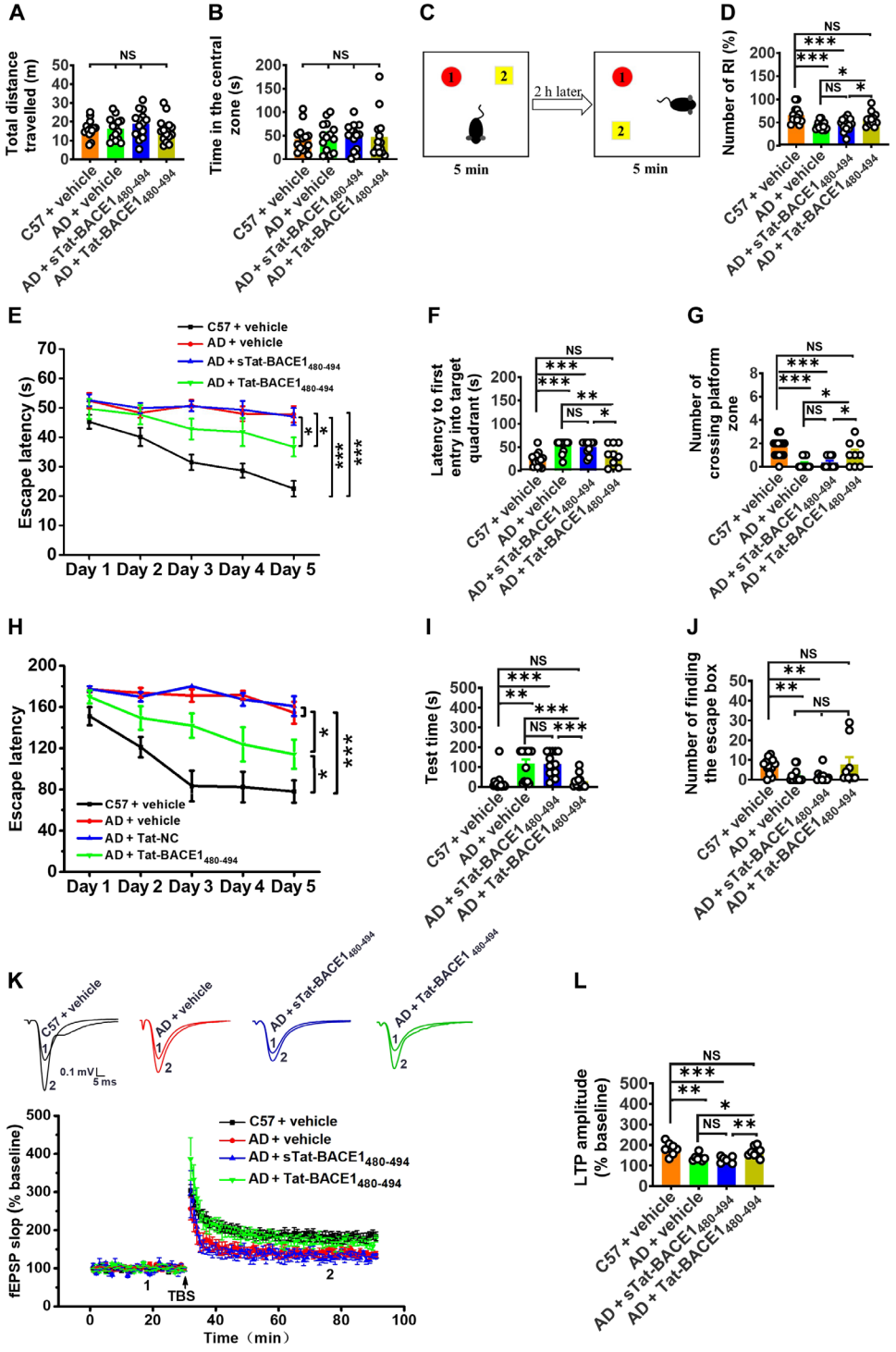

Fig. 4. Tat-BACE1$_{480-494}$ alleviates impairments in spatial memory and hippocampal CA1 LTP in AD model mice. (**A** and **B**) Effects of Tat-BACE1$_{480-494}$ on the spontaneous and anxiety-like behaviors in AD model mice in open-field test (n = 14 in each group). (**C** and **D**) Effects of Tat-BACE1$_{480-494}$ on the recognition index (RI) in AD model mice in novel object recognition test (n = 13 to 14 in each group). h, hours. (**E** to **G**) Effects of Tat-BACE1$_{480-494}$ on spatial learning and memory in AD model mice in the Morris water maze test (n = 9 to 14 in each group). (**H** to **J**) Effects of Tat-BACE1$_{480-494}$ on spatial learning and memory in AD model mice in the Barnes maze test (n = 13 to 14 in each group). (**K** and **L**) Effects of Tat-BACE1$_{480-494}$ on hippocampal CA1 LTP in AD model mice (n = 7 to 8 slices from three to four mice in each group). All data are expressed as means ± SEM. *P < 0.05; **P < 0.01; ***P < 0.001; not significant (NS). Statistical analyses were performed using two-way ANOVA (E and H) or one-way ANOVA followed by LSD multiple comparisons test for homogeneous variance or Dunnett's multiple comparisons test for heterogeneous variance (A, B, D, F, G, I, J, and L).

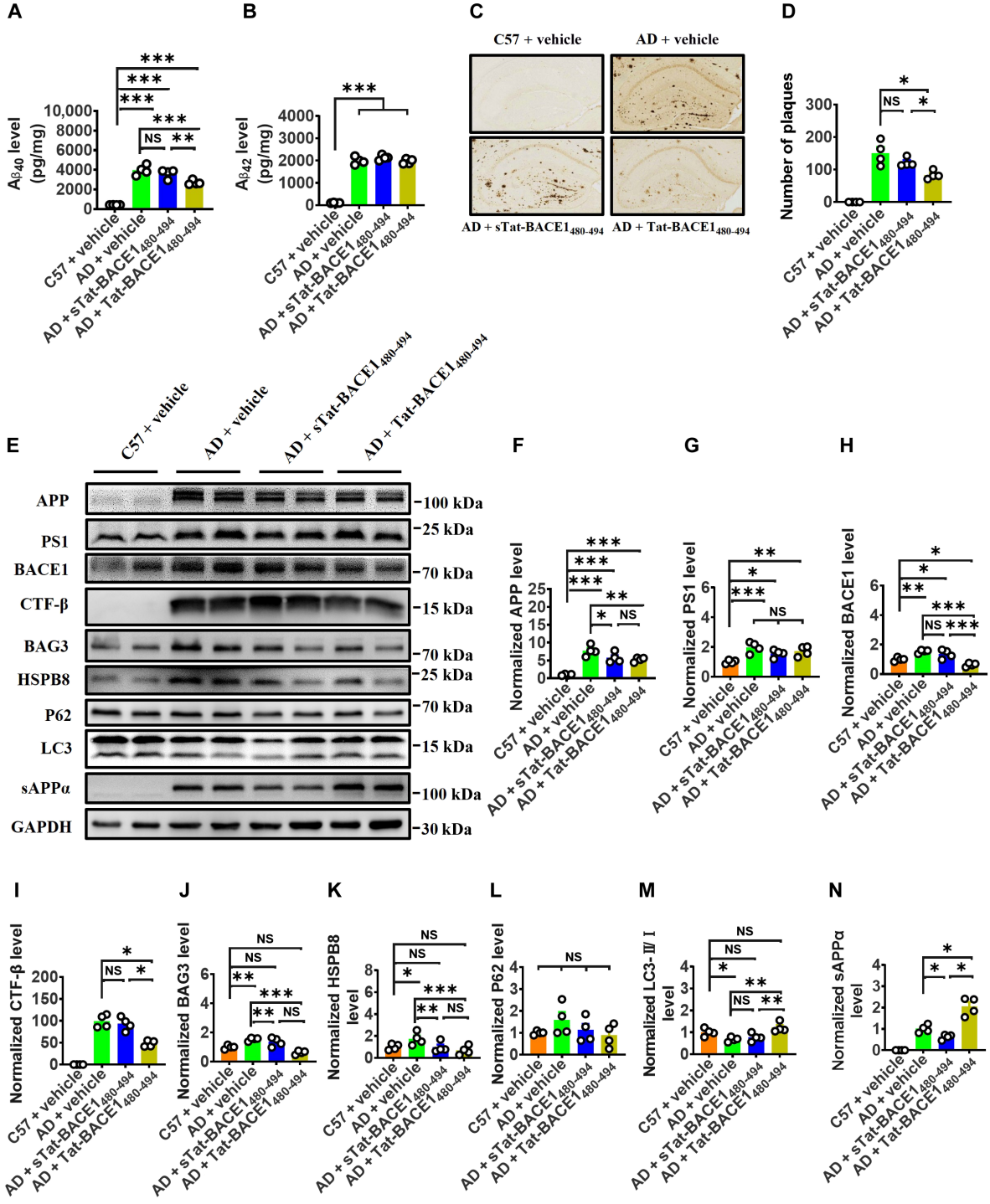

Fig. 5. Tat-BACE1$_{480\text{-}494}$ alleviates Aβ pathology in AD model mice. (**A** and **B**) Effects of Tat-BACE1$_{480\text{-}494}$ on Aβ$_{40}$ and Aβ$_{42}$ levels in the hippocampus of AD model mice ($n = 4$ in each group). (**C** and **D**) Effects of Tat-BACE1$_{480\text{-}494}$ on the formation of neuritic plaques in the hippocampus of AD model mice ($n = 4$ in each group). (**E** to **N**) Effects of Tat-BACE1$_{480\text{-}494}$ on protein levels of APP, PS1, BACE1, CTF-β, BAG3, HSPB8, P62, LC3-II/I, and sAPPα in the hippocampus of AD model mice aged 6 months ($n = 4$ in each group). All data are expressed as means ± SEM. *$P < 0.05$; **$P < 0.01$; ***$P < 0.001$; not significant (NS). Statistical analyses were performed using one-way ANOVA followed by LSD multiple comparisons test for homogeneous variance or Dunnett's multiple comparisons test for heterogeneous variance.

(Fig. 5, C and D). Because Aβ peptides are generated from APP by sequential cleavage by BACE1 and PS1, we next examined the expressions levels of APP and its cleaving enzymes. The results showed that Tat-BACE1$_{480\text{-}494}$ treatment significantly decreased APP and CTF-β levels while increasing sAPPα in the hippocampus of AD model mice (Fig. 5, E, F, I, and N). Moreover, BACE1 levels apparently reduced in the hippocampus of AD model mice treated with Tat-BACE1$_{480\text{-}494}$ (Fig. 5, E and H). Notably, neither Tat-BACE1$_{480\text{-}494}$ nor its scramble sTat-BACE1$_{480\text{-}494}$ affected PS1 levels in the hippocampus of AD model mice (Fig. 5, E and G). BAG3 and HSPB8 levels were simultaneously decreased in the hippocampus of AD model mice following treatment with sTat-BACE1$_{480\text{-}494}$ or Tat-BACE1$_{480\text{-}494}$ (Fig. 5, E, J, and K). Treatment with Tat-BACE1$_{480\text{-}494}$ resulted in an increase in LC3II/I ratio, while P62 levels remained unchanged, suggesting an improvement in autophagy in the hippocampus of AD mice (Fig. 5, E, L, and M). Together, these results suggest that Tat-BACE1$_{480\text{-}494}$ alleviates Aβ pathology through reducing BACE1 levels in AD model mice.

BAG3 knockdown alleviates Aβ pathology

To further validate the stabilizing effect of BAG3 on BACE1, we cultured and extracted primary neurons from AD double-transgenic mice and modulated BAG3 expression using lentivirus-mediated knockdown or overexpression. The results showed that APP and PS1 were highly expressed in the primary neurons of AD double transgenic mice (Fig. 6, A to C). BAG3 knockdown decreased BACE1, leading to a corresponding decrease in CTF-β levels. Although BAG3 overexpression increased BACE1 levels, it did not further elevate CTF-β (Fig. 6, A and F). However, neither BAG3 knockdown nor overexpression affected sAPPα, the α-cleaved product of APP (Fig. 6, A and G). In vivo, the CA1 region of the mouse hippocampus was injected with either a control virus (AAV$_{mScarlet}$) or an interfering virus (AAV$_{sh\text{-}BAG3}$) (Fig. 6H). The results showed that APP and PS1 were highly expressed in the hippocampus of AD double transgenic mice (Fig. 6, K to M). BAG3 knockdown did not affect APP and PS1 levels (Fig. 6, K to M) but significantly reduced BACE1 expression (Fig. 6, K, N, and O), leading to corresponding changes in CTF-β (Fig. 6, K and P) and Aβ$_{40}$ and Aβ$_{42}$ (Fig. 6, I and J). Consistent with the in vitro findings, BAG3 knockdown did not affect sAPPα levels in the hippocampus of AD mice (Fig. 6, K and Q).

DISCUSSION

The primary clinical manifestations of AD are impairments in cognition and memory functions, with pathological features typically appearing earliest and most prominently in the hippocampus. BACE1 serves as a key pathological factor in AD, highly expressed in the brain, and initiates APP amyloidogenic cleavage. The transmembrane domain of BACE1 is essential for its enzymatic activity and determines its subsequent Golgi localization and APP cleavage function. Phosphorylation of BACE1 at Ser^{498} leads to its recycling from endosome vesicles and relocation outside the Golgi apparatus, where it interacts with Golgi-localized gamma-ear-containing ARF-binding protein 1 to prevent BACE1 from trafficking to the cell surface and cleaving APP. Furthermore, phosphorylation at Thr^{252} significantly enhances the enzymatic activity of BACE1 (*41*). BACE1 can be categorized on the basis of the extent of *N*-glycosylation into immature proBACE1 and mature BACE1 (*42*). As a long-lived protein, the half-life of BACE1 is variably reported, ranging from 2 hours to possibly 12 hours, reflecting differing cells, experimental conditions, and contexts. Our focus has been on investigating the stability of endogenous BACE1, revealing that BAG3 can enhance BACE1 stability and maintain its expression after 48 hours (Fig. 2, S and U). Conditional knockout of BACE1 in adult 5xFAD mice can reverse amyloid deposition and improve LTP. However, it also reduces the cleavage of the neural cell adhesion protein CHL1, leading to axon guidance defects and structural disorganization of the mossy fiber pyramidal tract in the hippocampus, with its length reduced by ~30% (*43*, *44*). Now, most research efforts aimed at AD treatment drugs have been unsuccessful, with only two small-molecule BACE1 inhibitors remaining in clinical trials. Although traditional small-molecule BACE1 inhibitors effectively reduce Aβ levels in cerebrospinal fluid, they fail to improve or may even exacerbate cognitive decline. Except for MK8931, many of these inhibitors, such as AZD3293, LY2811376, AZD3839, LY2886721, PF-06751979, Inhibitor IV, and E2609, significantly prolong the half-life of BACE1 protein and lead to varying degrees of BACE1 protein accumulation in neurons (*45*). This phenomenon likely contributes to their ultimate lack of success in clinical trials for AD treatment. Compared to BACE1 knockout, small-molecule inhibitors primarily act by inhibiting BACE1 activity, exerting relatively minor effects on its physiological functions. However, their selectivity is lower than that of peptide-based drugs. Tat-BACE1$_{480\text{-}494}$ competitively disrupts the protein interaction between BAG3 and BACE1, demonstrating high specificity and enabling selective regulation of BACE1 protein levels. This approach may help mitigate or minimize synaptic disruptions.

BAG3 can be induced by multiple stress factors, which are significantly up-regulated in the prefrontal cortex, temporal cortex, and hippocampus of patients with AD. More than 60% of BAG3 mutation sites occur within the highly conserved BAG domain but with a low incidence rate that is unlikely to affect BAG3-HSP70 interaction (*46*–*48*). BAG3 stabilizes BACE1 through a ternary complex involving HSP70, termed the "HSP70-BAG3-BACE1" pattern. In the present study, we have identified the binding sites of BAG3 and BACE1, which are adjacent to and partially overlap with the IPV motif bound by HSPB8, potentially competitively inhibiting HSPB8 through BACE1 (fig. S3). Notably, the H109R mutation in the first IPV motif, where BAG3 binds to BACE1, leads to a dominant form of myopathy (*49*). However, its impact on AD pathology and the binding affinity between BACE1 and BAG3 remains unclear. The binding sites of BAG3-BACE1 rarely involve protein modification sites in BACE1, such as the *N*-glycosylation sites Asn^{153}, Asn^{172}, Asn^{223}, and Asn^{354} of proBACE1. Therefore, the interaction between BAG3 and BACE1 generally persists in normal or AD pathological states and is unlikely to inhibit the maturation of BACE1. Because the BACE1$_{I465\text{-}494A}$ region of BACE1 bound to BAG3 avoids the Ser^{498} and Thr^{252} sites, although BAG3 directly binds to and stabilizes BACE1, it is unlikely to affect the subcellular localization and β-secretase activity of BACE1 by interfering with the phosphorylation at Ser^{498} and Thr^{252} sites (fig. S5, A to D). Certainly, given the shared BACE1 binding sequence in proBACE1, BAG3 is also most likely to stabilize proBACE1 as well. Notably, the effects of BAG3 on other proteins related to AD, such as BACE2, ADAM10, and tau, are not involved in this study and further investigation on them is necessary in the future.

The binding site of human BACE1 to BAG3 is a 30–amino acid–long sequence, and the latter part overlaps partially with the binding site of BACE1 and RTN3. RTN3-BACE1 interaction reduces the stability of BACE1 and the production of Aβ (*50*), while BAG3 competes

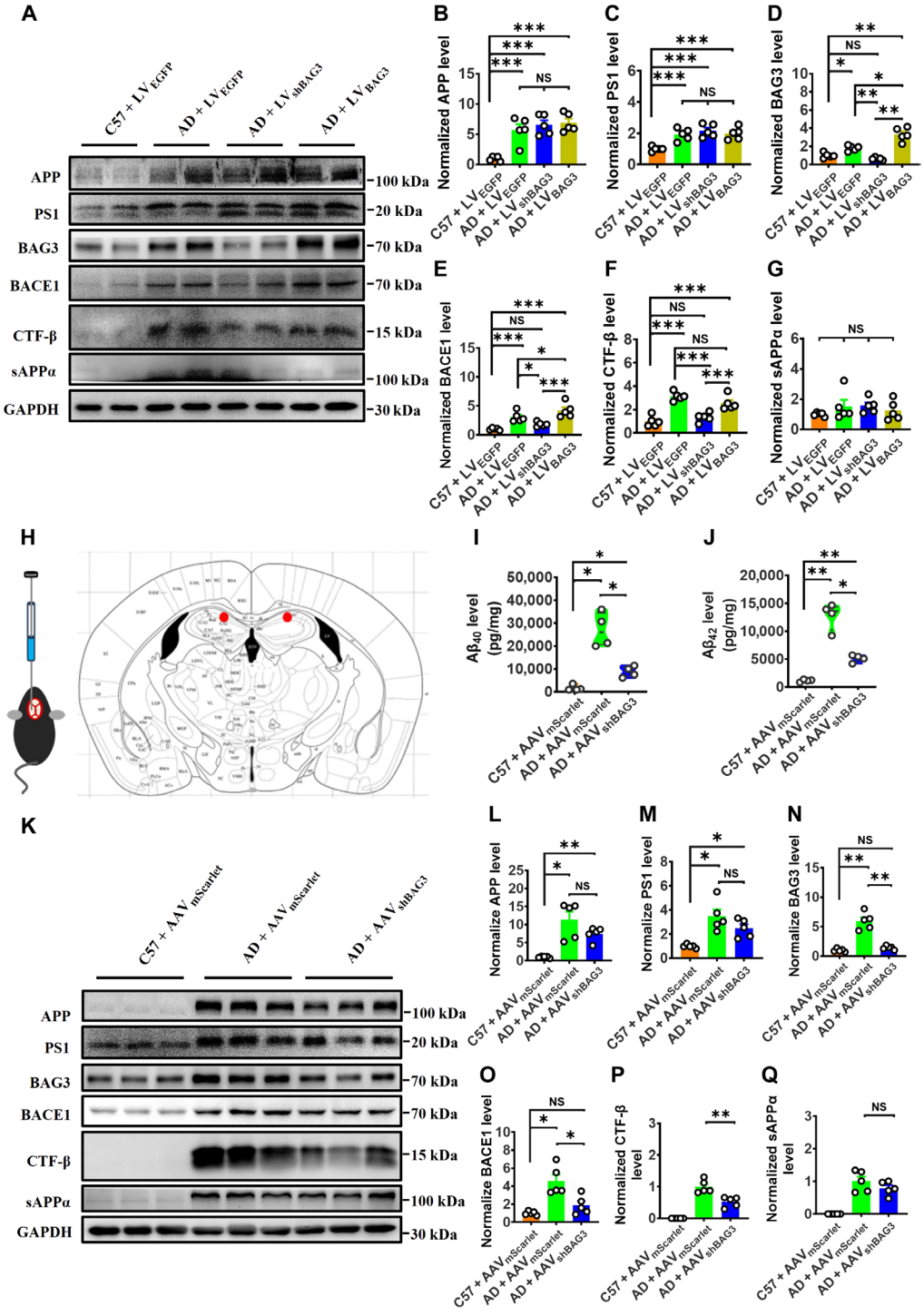

Fig. 6. BAG3 regulates Aβ pathology. (**A** to **G**) Protein levels of APP, PS1, BAG3, BACE1, CTF-β, and sAPPα in primary neurons from AD mice with BAG3 knockdown or overexpression ($n = 4$ in each group). (**H** to **J**) Levels of $A\beta_{40}$ and $A\beta_{42}$ in hippocampus of AD mice following BAG3 knockdown via adeno-associated virus (AAV; $n = 4$ in each group). (**K** to **Q**) Protein levels of APP, PS1, BAG3, BACE1, CTF-β, and sAPPα in the hippocampus of AD mice following BAG3 knockdown via AAV ($n = 5$ in each group). All data are expressed as means ± SEM. $^*P < 0.05$; $^{**}P < 0.01$; $^{***}P < 0.001$; not significant (NS). Statistical analyses were performed using a two-tailed unpaired Student's *t* test (P and Q) or one-way ANOVA followed by LSD multiple comparisons test for homogeneous variance or Dunnett's multiple comparisons test for heterogeneous variance (B to G, I, J, and L to O).

with RTN3 for the BACE1 binding site and stabilizes BACE1 through additional mechanisms. Although overexpression of RTN3 reduces Aβ production, it also causes notable neurite dystrophy, thus failing to improve the AD phenotype. Clearly, the role of RTN3 protein extends beyond BACE1 regulation, and it is not an ideal way to reduce BACE1 levels by regulating it. In contrast to proteins, short peptides offer high specificity and rapid action. On the basis of the BACE1-BAG3 binding site, we designed and synthesized Tat-BACE1$_{465\text{-}494}$, a 46–amino acid peptide with good water solubility, cell penetration, and effectiveness in competitively inhibiting the BAG3-BACE1 interaction. However, the length of Tat-BACE1$_{465\text{-}494}$ precludes its use as a peptide drug. Therefore, BACE1$_{480\text{-}494}$, located within the BACE1 binding region to RTN3 and with a smaller molecular weight, was synthesized. As expected, Tat-BACE1$_{480\text{-}494}$ effectively reduces the interaction between BAG3 and BACE1, thereby decreasing BACE1 levels and improving synaptic plasticity and memory in AD model mice (fig. S8, A and B; and Figs. 5H and 4, K and L). Thus, we believe that BACE1$_{480\text{-}494}$ is an effective fragment derived from BACE1$_{465\text{-}494}$, potentially serving as a safe and efficacious peptide drug for AD treatment.

We found that APP overexpression increased BAG3 in 20E2 (Fig. 1, S and V), whereas BACE1 overexpression, in contrast, reduced BAG3 levels in HEK293B2 (fig. S2, A and C). This suggests that APP may play an important role in inducing and even maintaining high BAG3 expression. Consequently, sTat-BACE1$_{480\text{-}494}$ treatment led to a reduction in APP levels (Fig. 5, E and F), which may, in turn, contribute to decreased BAG3 expression. Notably, although both sTat-BACE1$_{480\text{-}494}$ and Tat-BACE1$_{480\text{-}494}$ reduced BAG3 levels, only Tat-BACE1$_{480\text{-}494}$ effectively decreased BACE1. This discrepancy may be due to sTat-BACE1$_{480\text{-}494}$ being unable to disrupt the BAG3-BACE1 interaction. Additionally, we observed that sTat-BACE1$_{480\text{-}494}$ reduced HSPB8 levels to a similar extent as BAG3. Because the BAG3 binding site for BACE1 partially overlaps with its binding site for HSPB8 (fig. S3), the decrease in BAG3 levels may preferentially destabilize and downregulate HSPB8 (Fig. 2J). Compared with BAG3 genetic knockdown, the Tat-BACE1$_{480\text{-}494}$ peptide offers notable advantages. It not only inhibits the β-cleavage of APP, reducing CTF-β and Aβ production, but also promotes α-cleavage of APP, thereby lowering the overall APP burden. In summary, BAG3 directly binds to and stabilizes BACE1 through the HSP70-BAG3-BACE1 ternary complex. The peptide Tat-BACE1$_{480\text{-}494}$, developed on the basis of the BACE1-BAG3 binding site, effectively disrupts the interaction between BAG3 and BACE1 at their binding site. This disruption results in reduced BACE1, decreased Aβ generation, and, ultimately, improved synaptic plasticity and memory deficits in AD model mice (Fig. 7). Our findings provide compelling evidence supporting the development of BACE1-stabilizing inhibitors such as Tat-BACE1$_{480\text{-}494}$, as potential therapeutics for alleviating learning and memory impairments in patients with AD and aged populations. These properties highlight the great potential of Tat-BACE1$_{480\text{-}494}$ peptide for future clinical applications.

MATERIALS AND METHODS

Animals

APP23/PS45 double transgenic mice and their WT littermates were reproduced by in vitro fertilization at Cyagen Biosciences (Suzhou, China) and housed at the animal care center of Children's Hospital of Chongqing Medical University. The mice were maintained under a 12-hour light/dark cycle (7:00 a.m. to 7:00 p.m.) with free access to food and water in a temperature and humidity-controlled specific pathogen–free room. All animal experiments were performed according to Chongqing Science and Technology Commission guidelines and approved by the Ethics Committee of Children's Hospital of Chongqing Medical University (approval no. CHCMU-IACUC-20220323012).

Chemical reagents and antibodies

Anti-BAG3 (no. 10599-1-AP), anti-HSP70 (no. 10995-1-AP), anti-HSPB8 (no. 15287-1-AP), and anti-P62 (no. 18420-1-AP) antibodies were obtained from Proteintech Group Inc. (Wuhan, China). Anti-APP, anti-BACE1 (no. ab108394) and anti-PS1 (no. ab76083) antibodies were obtained from Abcam (Cambridge, UK). Anti-Tau antibody (no. AHB0042) was purchased from Invitrogen (San Diego, CA, USA). Anti–P-tau (S396; no. AF3148) and anti–P-tau (S404; no. AF3144) antibodies were obtained from Affinity Biosciences Co. Ltd. (Jiangsu, China). Anti-LC3A/B (no. CST12741) antibody was obtained from Cell Signaling Technology, Inc. (CST) (Danvers, MA, USA). Anti–glyceraldehyde-3-phosphate dehydrogenase antibody (no. ARG10112) was purchased from Arigo (Zhubei, Taiwan, China). Purified anti-Aβ, 17-24 antibody (4G8) (no. 800701) was purchased from BioLegend (San Diego, CA, USA). Anti-Flag immune magnetic beads (no. B26102) were purchased from Bimake (Houston, TX, USA). Pierce TM BCA Protein Assay Kit (no. 23225) was ordered from Thermo Fisher Scientific (Waltham, MA, USA). Cell Counting Kit-8 (CCK-8) assay kit (no. CA1210) was ordered from Solarbio (Beijing, China). Human $A\beta_{40}$ (no. DAB140B) and $A\beta_{42}$ (no. DAB142) Quantikine ELISA Kits were ordered from R&D Systems (Minneapolis, MN, USA).

Cell culture

HEK293, 20E2 (HEK293 cells stably transfected with human Swedish mutant APP695), 2EB2 (HEK293 stably transfected with human Swedish mutant APP695 and BACE1), HEK293B2 (HEK293 stably transfected with BACE1), HT22, and $N2A^{APP}$ (N2A stably transfected with human Swedish mutant APP695) cells were cultured with Dulbecco's modified Eagle's medium (DMEM) containing 10% fetal bovine serum (FBS). N2A cells were cultured with equivalent DMEM and Opti-MEM containing 5% FBS at 37°C in a humidified atmosphere containing 5% CO_2. 20E2 and $N2A^{APP}$ cells were incubated with G418. HEK293B2 cells were incubated with Zeocin, and 2EB2 cells were incubated with both G418 and Zeocin.

Cell viability assay

Using a microscope and cell counter, appropriate numbers of HEK293, N2A, and HT22 cells were seeded into 96-well plates with two to three replicate wells for each concentration. After allowing the cells to adhere and stabilize, an equal volume of saline or peptide was added to achieve final peptide concentrations of 0, 5, 10, 20, 40, 80, and 160 μM. The cells were then incubated for 24 hours. Following removal of the cell culture medium, a reaction solution was added to each well and incubated at 37°C for 1 hour. The optical density value was measured at a wavelength of 450 nm.

Western blotting

Cultured cells or mice hippocampal tissues were prepared and lysed on ice with radioimmunoprecipitation assay buffer containing protease and phosphatase inhibitors for 30 min. The lysates were then centrifuged at 14,000 rpm for 15 min at 4°C to collect the supernatants.

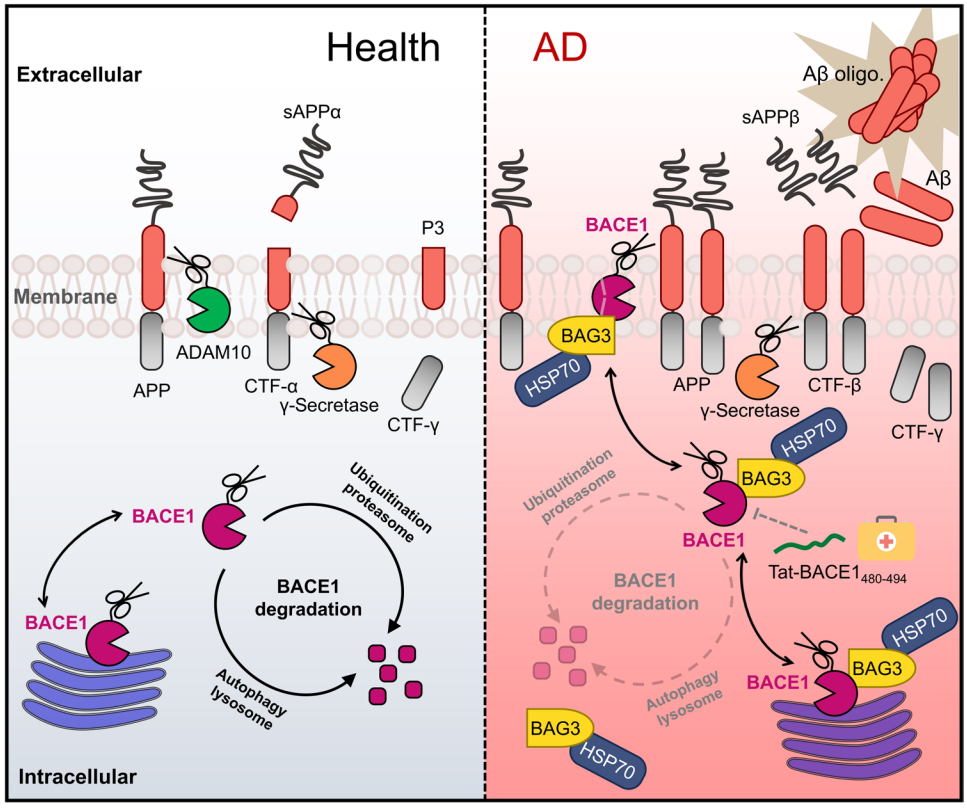

Fig. 7. The schematic illustrates the mechanism of Tat-BACE1$_{480-494}$ in AD. BAG3 directly binds and stabilizes BACE1 through forming the HSP70-BAG3-BACE1 ternary complex. BACE1$_{480-494}$ effectively disrupts the interaction between BAG3 and BACE1, consequently reducing BACE1 levels and Aβ generation in AD.

After determining the total protein concentration, protein samples were denatured with 5× sample buffer at 95°C for 5 min. Gel electrophoresis was performed using an appropriate voltage, and the proteins were transferred to a polyvinylidene difluoride (PVDF) membrane using 0.5× transfer buffer (or 1× transfer buffer for CTF-β, containing 10% methanol) at 160 mA for 140 min (or 200 mA for CTF-β for 30 min) at 4°C. Subsequently, the PVDF membranes were blocked with 10% skim milk for 60 to 90 min at room temperature. Next, the PVDF membranes were incubated with the primary antibodies overnight at 4°C. The following day, the membranes were incubated with corresponding horseradish peroxidase–labeled goat anti-rabbit immunoglobulin G (IgG) or goat anti-mouse IgG antibodies for 60 to 120 min at room temperature. Last, the immunoblots were visualized by exposing the PVDF membranes to Western Enhanced ChemiLuminescence (ECL) substrate and imaging using a Bio-Rad Imager. Data collection was performed using Quantity One software.

Co-immunoprecipitation

The cells were scraped off and lysed on ice for 30 min using Western and immunoprecipitation lysis buffer supplemented with protease inhibitors. The lysate was then centrifuged at 12,000 rpm for 20 min at 4°C to collect the supernatants. After removing background binding with magnetic beads, the protein concentration was determined by using a Bicinchoninic Acid (BCA) protein assay kit. Primary antibodies or nonspecific IgG were added to 300 to 1500 μg of protein samples and mixed overnight at 4°C. The next day, the mixture was further mixed with 25 to 50 μl of protein A/G beads for an additional 2 hours at 4°C. The beads were separated using a magnetic frame and washed four times with ice-cold PBS. The proteins bound on beads were eluted by boiling in 1× sample buffer for more than 5 min at 95°C and lastly analyzed by Western blotting.

Enzyme-linked immunosorbent assay

The enzyme-linked immunosorbent assay was used to quantify the levels of $A\beta_{40}$ and $A\beta_{42}$ in the hippocampus. The 96-well plate was first washed with wash buffer. Subsequently, 100 μl of standards, controls, and samples were added into the respective wells. The plate was then sealed and incubated at 2° to 8°C for 2 hours. After incubation, the wells were washed again with wash buffer. Next, 200 μl of cold Aβ conjugate was added to each well the plate was sealed and incubated at 2° to 8°C for additional 2 hours. Following another round of washing with wash buffer, 200 μl of substrate solution was added to each well. The plate was then incubated in the dark at room temperature for 30 min. Last, 50 μl of stop solution was added to each well to halt the reaction, and the absorbance of the wells was measured at a wavelength of 450 nm within 30 min.

Immunohistochemistry

After anesthetizing, the mouse brain was dissected and fixed with 4% paraformaldehyde at 4°C for over 24 hours. Following fixation, the brains were dehydrated overnight in a 30% sucrose solution at 4°C. Subsequently, the brains were embedded in optimal cutting temperature (OCT) and cryosectioned at −20°C. The brain sections were selected and washed with 1× PBST (0.3% Triton X-100 in 1×

PBS). Then, the sections were incubated with 88% formic acid for 10 to 15 min to enhance antigen retrieval. After another round of washing with 1× PBST again, the sections were treated with 0.5% H_2O_2 for 30 min at room temperature to block endogenous peroxidase activity. Following a wash with 1× PBST, the sections were blocked with 10% bovine serum albumin for 1 hour to prevent nonspecific binding. The brain sections were then incubated overnight at 4°C with 4G8 primary antibody (1:500) to detect Aβ plaques. After washing with 1× PBST, the sections were incubated with an Avidin–Biotin Complex (ABC) solution at 37°C for 1 hour. Subsequently, they were washed again with 1× PBST and stained with diaminobenzidine (DAB) for 10 to 15 min at room temperature in a dark environment. Following DAB staining, the sections were washed with 1× PBST. Once the brain sections on slides were slightly dry, they underwent gradient dehydration with 75%, 85%, and absolute ethanol, followed by transparentizing with OT transparent agent xylene. Last, the sections were sealed with neutral resin for long-term preservation. The number of neuritic plaques was quantified using microscopy as previously described (*51*).

Peptide array assay

The BAG3 and BACE1 peptide array membranes were designed and synthesized based on human sequences. Each spot on the membrane contained a 12–amino acid peptide segment, with each subsequent spot moving 2 amino acids backward from the previous one. To initiate the interaction study, the BAG3 or BACE1 peptide array membrane was individually exposed to purified human BACE1 or BAG3 protein (1 μg/ml), respectively. Following protein incubation, the membranes were subjected to Western blotting using an ECL substrate and subsequently imaged using a Bio-Rad Imager. A positive interaction between BAG3 and BACE1 is indicated by the presence of three or more consecutive positive spots on the peptide array membrane.

Open-field test

After 90 days of peptide administration, an open-field test was carried out to assess the general motor abilities and anxiety-like behavior of mice. Each mouse was placed in an open box measuring 40 cm by 40 cm by 60 cm, released from the central area, and allowed to explore freely for 10 min. The data were recorded and analyzed using ANY-maze video tracking system (Stoelting, USA).

Novel object recognition test

Following the open-field test, the mice were subjected to a novel object recognition test. The mice were placed in the same open box (40 cm by 40 cm by 60 cm) facing two identical objects fixed on the floor and allowed to explore freely for 5 min. Then, the mice were returned to their home cages, and one of the objects was moved to a different location after an interval of 1 hour. The mice were reintroduced to the box and allowed to freely explore for another 5 min to test their ability to recognize the novel object. The number and during of contact with the new object were recorded and analyzed using ANY-maze video tracking system (Stoelting, USA). The RI = (the number or time of head contacts with the novel object/total number or time of head contacts with both objects) × 100%.

Barnes maze test

The maze consists of a white circular platform with a diameter of 0.75 m, and 18 holes (5 cm in diameter) evenly distributed along the edge, with one hole containing an escape box underneath (*52*). During the habituation phase, mice were allowed to freely explore the maze without an escape box for 3 min. During the subsequent 5-day training stage, mice underwent two spatial learning trials each day. If a mouse successfully entered the escape box within 3 min, then the trial was completed. If a mouse failed to find the escape box within 3 min, then it was gently guided to the escape box, where it remained for 60 s before being returned to its home cage. On day 7, a probe test was conducted, during which each mouse was tested for 3 min to assess its spatial memory and navigation ability. All data were recorded and analyzed using ANY-maze video tracking system (Stoelting, USA).

Morris water maze test

The maze consists of a circular water tank with a diameter of 150 cm and a height of 60 cm. The tank is divided into four quadrants: northeast (NE) (quadrant 1), northwest (NW) (quadrant 2), southwest (SW) (quadrant 3), and southeast (SE) (quadrant 4). The experimental protocol was divided into three stages: adaptation, training, and probe test. During the adaptation phase, the mice were gently placed in the water from the first quadrant, facing the pool wall, and allowed to freely explore the pool for 2 min. During the training stage, a white cylindrical platform (7.5 cm in diameter) was positioned at the center of the third quadrant of the maze, with its top 1 cm below the water surface. The mice underwent continuous training for 5 days, with four trials conducted each day. For each trial, mice were gently placed into the water from different quadrants, facing the pool wall. If a mouse found the hidden platform within 60 s and remained on it for more than 2 s, then the trial was considered successful, and the time taken to find the platform (escape latency) was recorded. If a mouse failed to find the platform within 60 s, then it was gently guide to the platform and allowed to stay there for 20 s. During the probe test, the mice were placed into water from the first quadrant and allowed to freely explore for 60 s, with the hidden platform removed. The swim path was recorded and analyzed using ANY-maze video tracking system (Stoelting, USA).

Electrophysiological recording

As previously described (*53*), mice were deeply anesthetized with urethane (1.5 g/kg, ip) and infused with hypertonic artificial cerebrospinal fluid (ACSF) [3.0 mM KCl, 1.25 mM $NaH_2PO_4.H_2O$, 26 mM $NaHCO_3$, 0.4 mM Na–vitamin C, 2.0 mM pyruvate-Na, 2.0 mM, 10.0 mM D-glucose, 220 mM sucrose, 0.1 mM $CaCl_2$, 2.0 mM $MgCl_2$, and 4.0 mM $MgSO_4$ (pH 7.4)] through the heart, and the brains were quickly removed after decapitation. Then, coronal hippocampal slices (400 μm) were performed in hypertonic solution with 95% O_2 and 5% CO_2 using a vibratome (VT1200S, Leica Microsystems, Germany). Before recording, the hippocampal slices were incubated in normal ACSF containing [124 mM NaCl, 2.8 mM KCl, 1.25 mM $NaH_2PO_4.H_2O$, 2.0 mM $CaCl_2$, 1.2 mM $MgSO_4$, 0.4 mM Na–vitamin C, 26 mM $NaHCO_3$, 2.0 mM Na-lactate, 2.0 mM pyruvate-Na, and 10.0 mM D-glucose (pH 7.4)] bubbled with 95% O_2 and 5% CO_2 at 35°C for 2 hours to facilitate recovery. A concentric bipolar stimulating electrode was placed in the Schaffer branch of the dorsal hippocampal CA3 pyramidal neurons, and a glass microelectrode filled with normal ASCF was placed in the radial striatum of the hippocampal CA1 area. The excitatory postsynaptic potentials (EPSPs) were induced at a frequency of 0.05 Hz, and the stimulus intensity was adjusted to ~50% of the maximum EPSPs slope. After obtaining a baseline for 30 min. LTP was induced by theta burst stimulation, which consisted of two trains of stimuli (at 20-s interval), with each

train composed of five bursts (four pulses at 100 Hz in each burst) at an inter-burst interval of 200 ms. Data collection was carried out using PatchMaster v2.73 software (Lambrecht/Pfalz HEKA Elektronik, Germany).

Primary neuron processing

APP and PS1 single-transgenic mice were crossed, and embryos at 16 to 18 days of gestation were collected. The brains were isolated, the meninges were removed, and primary neurons were obtained through enzymatic digestion. The remaining brain tissues were used for genotyping. Primer sequence: APP1082 (5′-CTTGACGTTCTGCCTCTTCC-3′), PS-1 (5′-ATCACAGCCAAGATGAGC-3′), and Thy1E2 (5′-CACCACAGAATCCAAGTCGG-3′). On the sixth day of culture, WT primary neurons were treated with the control lentivirus (LV_{EGFP}), while APP23/PS45 primary neurons were treated with either LV_{EGFP}, the interfering lentivirus (LV_{shBAG3}), or the overexpression lentivirus (LV_{BAG3}). After an additional 4 days of culture, proteins were extracted for analysis.

Adeno-associated virus and stereotaxic injection

AAV_{shBAG3} (sequence: gaAGGCAAGAAGACTGATAAA) and its control virus $AAV_{mScarlet}$ were constructed by OBiO Technology (Shanghai, China) and microinjected into the CA1 region of the mouse hippocampus (−2.5 mm posterior, ±2.0 mm lateral, and 2.5 mm ventral relative to bregma) (*54*).

Statistical analysis

All data were expressed as means ± SEM. For comparisons between two groups, a two-tailed Student's *t* test was used. For comparisons among more than two groups, analysis of variance (ANOVA) was performed. Data from spatial learning tasks in the Barnes maze and Morris water maze were analyzed using two-way ANOVA, with group as the between-subject factor and with training trials as the within-subject factor. Other data were analyzed using one-way ANOVA. Statistical significance was defined as follows: $^{*}P < 0.05$; $^{**}P < 0.01$; $^{***}P < 0.001$; not significant (NS). All data obtained through biological replicates.

Supplementary Materials

This PDF file includes:

Figs. S1 to S12

Tables S1 and S2

REFERENCES AND NOTES

1. C. L. Masters, R. Bateman, K. Blennow, C. C. Rowe, R. A. Sperling, J. L. Cummings, Alzheimer's disease. *Nat. Rev. Dis. Primers* **1**, 15056 (2015).
2. S. Lammich, E. Kojro, R. Postina, S. Gilbert, R. Pfeiffer, M. Jasionowski, C. Haass, F. Fahrenholz, Constitutive and regulated alpha-secretase cleavage of Alzheimer's amyloid precursor protein by a disintegrin metalloprotease. *Proc. Natl. Acad. Sci. U.S.A.* **96**, 3922–3927 (1999).
3. R. Vassar, BACE1: The beta-secretase enzyme in Alzheimer's disease. *J. Mol. Neurosci.* **23**, 105–114 (2004).
4. H. A. Taylor, L. Przemylska, E. M. Clavane, P. J. Meakin, BACE1: More than just a β-secretase. *Obes. Rev.* **23**, e13430 (2022).
5. B. Das, R. Yan, A close look at BACE1 inhibitors for Alzheimer's disease treatment. *CNS Drugs* **33**, 251–263 (2019).
6. K. Zhu, X. Xiang, S. Filser, P. Marinković, M. M. Dorostkar, S. Crux, U. Neumann, D. R. Shimshek, G. Rammes, C. Haass, S. F. Lichtenthaler, J. M. Gunnersen, J. Herms, Beta-site amyloid precursor protein cleaving enzyme 1 inhibition impairs synaptic plasticity via seizure protein 6. *Biol. Psychiatry* **83**, 428–437 (2018).
7. E. McDade, I. Voytyuk, P. Aisen, R. J. Bateman, M. C. Carrillo, B. De Strooper, C. Haass, E. M. Reiman, R. Sperling, P. N. Tariot, R. Yan, C. L. Masters, R. Vassar, S. F. Lichtenthaler, The case for low-level BACE1 inhibition for the prevention of Alzheimer disease. *Nat. Rev. Neurol.* **17**, 703–714 (2021).
8. J. S. Choi, J. H. Lee, H. Y. Kim, M. H. Chun, J. W. Chung, M. Y. Lee, Developmental expression of Bis protein in the cerebral cortex and hippocampus of rats. *Brain Res.* **1092**, 69–78 (2006).
9. F. Domínguez, S. Cuenca, Z. Bilińska, R. Toro, E. Villard, R. Barriales-Villa, J. P. Ochoa, F. Asselbergs, A. Sammani, M. Franaszczyk, M. Akhtar, M. J. Coronado-Albi, D. Rangel-Sousa, J. F. Rodriguez-Palomares, J. Jiménez-Jáimez, J. M. Garcia-Pinilla, T. Ripoll-Vera, M. V. Mogollón-Jiménez, A. Fontalba-Romero, D. Garcia-Medina, J. Palomino-Doza, D. de Gonzalo-Calvo, M. Cicerchia, J. Salazar-Mendiguchia, C. Salas, S. Pankuweit, T. M. Hey, J. Mogensen, P. J. Barton, P. Charron, P. Elliott, P. Garcia-Pavia, European Genetic Cardiomyopathies Initiative Investigators, Dilated cardiomyopathy due to BLC2-associated athanogene 3 (BAG3) mutations. *J. Am. Coll. Cardiol.* **72**, 2471–2481 (2018).
10. J. A. Kirk, J. Y. Cheung, A. M. Feldman, Therapeutic targeting of BAG3: Considering its complexity in cancer and heart disease. *J. Clin. Invest.* **131**, e149415 (2021).
11. A. B. Meriin, A. Narayanan, L. Meng, I. Alexandrov, X. Varelas, I. I. Cissé, M. Y. Sherman, Hsp70-Bag3 complex is a hub for proteotoxicity-induced signaling that controls protein aggregation. *Proc. Natl. Acad. Sci. U.S.A.* **115**, E7043–E7052 (2018).
12. M. Fuchs, D. J. Poirier, S. J. Seguin, H. Lambert, S. Carra, S. J. Charette, J. Landry, Identification of the key structural motifs involved in HspB8/HspB6–Bag3 interaction. *Biochem. J.* **425**, 245–255 (2009).
13. Z. Xu, K. Graham, M. Foote, F. Liang, R. Rizkallah, M. Hurt, Y. Wang, Y. Wu, Y. Zhou, 14-3-3 protein targets misfolded chaperone-associated proteins to aggresomes. *J. Cell Sci.* **126**, 4173–4186 (2013).
14. C. Behl, Breaking BAG: The co-chaperone BAG3 in health and disease. *Trends Pharmacol. Sci.* **37**, 672–688 (2016).
15. C. Behl, BAG3 and friends: Co-chaperones in selective autophagy during aging and disease. *Autophagy* **7**, 795–798 (2011).
16. B. Tedesco, L. Vendredy, V. Timmerman, A. Poletti, The chaperone-assisted selective autophagy complex dynamics and dysfunctions. *Autophagy* **19**, 1619–1641 (2023).
17. P. W. Sheehan, C. J. Nadarajah, M. F. Kanan, J. N. Patterson, B. Novotny, J. H. Lawrence, M. W. King, L. Brase, C. E. Inman, C. M. Yuede, J. Lee, T. K. Patel, O. Harari, B. A. Benitez, A. A. Davis, E. S. Musiek, An astrocyte BMAL1-BAG3 axis protects against alpha-synuclein and tau pathology. *Neuron* **111**, 2383–2398.e7 (2023).
18. M. Gamerdinger, P. Hajieva, A. M. Kaya, U. Wolfrum, F. U. Hartl, C. Behl, Protein quality control during aging involves recruitment of the macroautophagy pathway by BAG3. *EMBO J.* **28**, 889–901 (2009).
19. J. Zhou, H. M. Chow, Y. Liu, D. Wu, M. Shi, J. Li, L. Wen, Y. Gao, G. Chen, K. Zhuang, H. Lin, G. Zhang, W. Xie, H. Li, L. Leng, M. Wang, N. Zheng, H. Sun, Y. Zhao, Y. Zhang, M. Xue, T. Y. Huang, G. Bu, H. Xu, Z. Yuan, K. Herrup, J. Zhang, Cyclin-dependent kinase 5-dependent BAG3 degradation modulates synaptic protein turnover. *Biol. Psychiatry* **87**, 756–769 (2020).
20. M. Y. Lee, S. Y. Kim, S. L. Shin, Y. S. Choi, J. H. Lee, Y. Tsujimoto, J. H. Lee, Reactive astrocytes express bis, a bcl-2-binding protein, after transient forebrain ischemia. *Exp. Neurol.* **175**, 338–346 (2002).
21. D. Avramopoulos, M. Szymanski, R. Wang, S. Bassett, Gene expression reveals overlap between normal aging and Alzheimer's disease genes. *Neurobiol. Aging* **32**, 2319. e27–2319.e34 (2010).
22. K. Seidel, J. Vinet, W. F. A. den Dunnen, E. R. Brunt, M. Meister, A. Boncoraglio, M. P. Zijlstra, H. W. G. M. Boddeke, U. Rüb, H. H. Kampinga, S. Carra, The HSPB8-BAG3 chaperone complex is upregulated in astrocytes in the human brain affected by protein aggregation diseases. *Neuropathol. Appl. Neurobiol.* **38**, 39–53 (2012).
23. V. Astillero-Lopez, M. Gonzalez-Rodriguez, S. Villar-Conde, A. Flores-Cuadrado, A. Martinez-Marcos, I. Ubeda-Banon, D. Saiz-Sanchez, Neurodegeneration and astrogliosis in the entorhinal cortex in Alzheimer's disease: Stereological layer-specific assessment and proteomic analysis. *Alzheimers Dement.* **18**, 2468–2480 (2022).
24. M. G. Tan, W. T. Chua, M. M. Esiri, A. D. Smith, H. V. Vinters, M. K. Lai, Genome wide profiling of altered gene expression in the neocortex of Alzheimer's disease. *J. Neurosci. Res.* **88**, 1157–1169 (2010).
25. M. Gonzalez-Rodriguez, S. Villar-Conde, V. Astillero-Lopez, P. Villanueva-Anguita, I. Ubeda-Banon, A. Flores-Cuadrado, A. Martinez-Marcos, D. Saiz-Sanchez, Neurodegeneration and astrogliosis in the human CA1 hippocampal subfield are related to hsp90ab1 and bag3 in Alzheimer's disease. *Int. J. Mol. Sci.* **23**, 165 (2021).
26. R. Li, K. Lindholm, L.-B. Yang, X. Yue, M. Citron, R. Yan, T. Beach, L. Sue, M. Sabbagh, H. Cai, P. Wong, D. Price, Y. Shen, Amyloid beta peptide load is correlated with increased beta-secretase activity in sporadic Alzheimer's disease patients. *Proc. Natl. Acad. Sci. U.S.A.* **101**, 3632–3637 (2004).
27. L.-B. Yang, K. Lindholm, R. Yan, M. Citron, W. Xia, X.-L. Yang, T. Beach, L. Sue, P. Wong, D. Price, R. Li, Y. Shen, Elevated beta-secretase expression and enzymatic activity detected in sporadic Alzheimer disease. *Nat. Med.* **9**, 3–4 (2003).
28. J. N. Rauch, J. E. Gestwicki, Binding of human nucleotide exchange factors to heat shock protein 70 (Hsp70) generates functionally distinct complexes in vitro. *J. Biol. Chem.* **289**, 1402–1414 (2014).

29. W. Mizushima, J. Sadoshima, BAG3 plays a central role in proteostasis in the heart. *J. Clin. Invest.* **127**, 2900–2903 (2017).
30. X. Fang, J. Bogomolovas, T. Wu, W. Zhang, C. Liu, J. Veevers, M. J. Stroud, Z. Zhang, X. Ma, Y. Mu, D. H. Lao, N. D. Dalton, Y. Gu, C. Wang, M. Wang, Y. Liang, S. Lange, K. Ouyang, K. L. Peterson, S. M. Evans, J. Chen, Loss-of-function mutations in co-chaperone BAG3 destabilize small HSPs and cause cardiomyopathy. *J. Clin. Invest.* **127**, 3189–3200 (2017).
31. C. N. Im, H. H. Yun, B. Song, D. Y. Youn, M. N. Cui, H. S. Kim, G. S. Park, J. H. Lee, BIS-mediated STAT3 stabilization regulates glioblastoma stem cell-like phenotypes. *Oncotarget* **7**, 35056–35070 (2016).
32. S. Habata, M. Iwasaki, A. Sugio, M. Suzuki, M. Tamate, S. Satohisa, R. Tanaka, T. Saito, BAG3-mediated Mcl-1 stabilization contributes to drug resistance via interaction with USP9X in ovarian cancer. *Int. J. Oncol.* **49**, 402–410 (2016).
33. S. Zhao, J. M. Wang, J. Yan, D. L. Zhang, B. Q. Liu, J. Y. Jiang, C. Li, S. Li, X. N. Meng, H. Q. Wang, BAG3 promotes autophagy and glutaminolysis via stabilizing glutaminase. *Cell Death Dis.* **10**, 284 (2019).
34. N. Chanana, U. Pati, ORP150-CHIP chaperone antagonism control BACE1-mediated amyloid processing. *J. Cell. Biochem.* **119**, 4615–4626 (2018).
35. H. Qing, W. Zhou, M. A. Christensen, X. Sun, Y. Tong, W. Song, Degradation of BACE by the ubiquitin-proteasome pathway. *FASEB J.* **18**, 1571–1573 (2004).
36. T. Feng, P. Tammineni, C. Agrawal, Y. Y. Jeong, Q. Cai, Autophagy-mediated regulation of BACE1 protein trafficking and degradation. *J. Biol. Chem.* **292**, 1679–1690 (2017).
37. A. Gentilella, K. Khalili, BAG3 expression in glioblastoma cells promotes accumulation of ubiquitinated clients in an Hsp70-dependent manner. *J. Biol. Chem.* **286**, 9205–9215 (2011).
38. Q. Shi, Y. Ge, M. G. Sharoar, W. He, R. Xiang, Z. Zhang, X. Hu, R. Yan, Impact of RTN3 deficiency on expression of BACE1 and amyloid deposition. *J. Neurosci.* **34**, 13954–13962 (2014).
39. W. He, Q. Shi, X. Hu, R. Yan, The membrane topology of RTN3 and its effect on binding of RTN3 to BACE1. *J. Biol. Chem.* **282**, 29144–29151 (2007).
40. H. S. Gns, S. G. Rajalekshmi, R. R. Burri, Revelation of pivotal genes pertinent to Alzheimer's pathogenesis: A methodical evaluation of 32 GEO datasets. *J. Mol. Neurosci.* **72**, 303–322 (2022).
41. W. J. Song, M. Y. Son, H. W. Lee, H. Seo, J. H. Kim, S. H. Chung, Enhancement of BACE1 activity by p25/Cdk5-mediated phosphorylation in Alzheimer's disease. *PLOS ONE* **10**, e0136950 (2015).
42. M. Haniu, P. Denis, Y. Young, E. A. Mendiaz, J. Fuller, J. O. Hui, B. D. Bennett, S. Kahn, S. Ross, T. Burgess, V. Katta, G. Rogers, R. Vassar, M. Citron, Characterization of Alzheimer's β-secretase protein BACE. A pepsin family member with unusual properties. *J. Biol. Chem.* **275**, 21099–21106 (2000).
43. M. H. Ou-Yang, J. E. Kurz, T. Nomura, J. Popovic, T. W. Rajapaksha, H. Dong, A. Contractor, D. M. Chetkovich, W. G. Tourtellotte, R. Vassar, Axonal organization defects in the hippocampus of adult conditional BACE1 knockout mice. *Sci. Transl. Med.* **10**, eaao5620 (2018).
44. X. Hu, B. Das, H. Hou, W. He, R. Yan, BACE1 deletion in the adult mouse reverses preformed amyloid deposition and improves cognitive functions. *J. Exp. Med.* **215**, 927–940 (2018).
45. L. Liu, B. M. Lauro, L. Ding, M. Rovere, M. S. Wolfe, D. J. Selkoe, Multiple BACE1 inhibitors abnormally increase the BACE1 protein level in neurons by prolonging its half-life. *Alzheimers Dement.* **15**, 1183–1194 (2019).
46. E. Sturner, C. Behl, The role of the multifunctional BAG3 protein in cellular protein quality control and in disease. *Front. Mol. Neurosci.* **10**, 177 (2017).
47. A. Arakawa, N. Handa, N. Ohsawa, M. Shida, T. Kigawa, F. Hayashi, M. Shirouzu, S. Yokoyama, The C-terminal BAG domain of BAG5 induces conformational changes of the Hsp70 nucleotide-binding domain for ADP-ATP exchange. *Structure* **18**, 309–319 (2010).
48. H. Sondermann, C. Scheufler, C. Schneider, J. Hohfeld, F. U. Hartl, I. Moarefi, Structure of a Bag/Hsc70 complex: Convergent functional evolution of Hsp70 nucleotide exchange factors. *Science* **291**, 1553–1557 (2001).
49. M. Meister-Broekema, R. Freilich, C. Jagadeesan, J. N. Rauch, R. Bengoechea, W. W. Motley, E. F. E. Kuiper, M. Minoia, G. V. Furtado, M. A. W. H. van Waarde, S. J. Bird, A. Rebelo, S. Zuchner, P. Pytel, S. S. Scherer, F. F. Morelli, S. Carra, C. C. Weihl, S. Bergink, J. E. Gestwicki, H. H. Kampinga, Myopathy associated BAG3 mutations lead to protein aggregation by stalling Hsp70 networks. *Nat. Commun.* **9**, 5342 (2018).
50. Q. Shi, M. Prior, W. He, X. Tang, X. Hu, R. Yan, Reduced amyloid deposition in mice overexpressing RTN3 is adversely affected by preformed dystrophic neurites. *J. Neurosci.* **29**, 9163–9173 (2009).
51. M. Luo, Y. Pang, J. Li, L. Yi, B. Wu, Q. Tian, Y. He, M. Wang, L. Xia, G. He, W. Song, Y. Du, Z. Dong, miR-429-3p mediates memory decline by targeting MKP-1 to reduce surface GluA1-containing AMPA receptors in a mouse model of Alzheimer's disease. *Acta Pharm. Sin. B* **14**, 635–652 (2024).
52. L. Xia, Y. Pang, J. Li, B. Wu, Y. Du, Y. Chen, M. Luo, Y. Wang, Z. Dong, Dihydroartemisinin induces O-GlcNAcylation and improves cognitive function in a mouse model of tauopathy. *J. Alzheimers Dis.* **84**, 239–248 (2021).
53. J. Li, Y. Pang, Y. Du, L. Xia, M. Chen, Y. Fan, Z. Dong, Lack of interferon regulatory factor 3 leads to anxiety/depression-like behaviors through disrupting the balance of neuronal excitation and inhibition in mice. *Genes Dis.* **10**, 1062–1074 (2023).
54. Y. Du, M. Fu, Z. Huang, X. Tian, J. Li, Y. Pang, W. Song, Y. Tian Wang, Z. Dong, TRPV1 activation alleviates cognitive and synaptic plasticity impairments through inhibiting AMPAR endocytosis in APP23/PS45 mouse model of Alzheimer's disease. *Aging Cell* **19**, e13113 (2020).

Acknowledgments: We would like to express our special thanks to L. Yi, C. Dai, and all other members in the Dong lab for helpful discussions and technical support. **Funding:** This work was supported by the National Natural Science Foundation of China (32371030, 82371194, and 82101466), the Natural Science Foundation of Chongqing (CSTB2024NSCQ-LZX0008 and CSTB2022NSCQ-LZX0010), and CQMU Program for Youth Innovation in Future Medicine (W0044). **Author contributions:** L.X., Y.D., C.C., Y.T.W., W.S., and Z.D. conceived of the original concept of this study. L.X., J.L., M.X., Q.T., B.W., and Z.D. contributed to design of methodology. M.X. and Y.Q. contributed to computer programs. Y.P., C.D., M.X., M.C., W.S., and Z.D. contributed to the verification of reproducibility of experimental results. L.X., C.D., M.X., and Z.D. analyzed experimental data. J.L., Y.P., C.D., M.X., Q.T., B.W., Y.Q., and C.C. conducted investigation process. L.X., C.D., L.Y., M.C., C.C., Y.T.W., W.S., and Z.D. provided study materials. Z.D. contributed to data curation. L.X., Y.Q., and Z.D. wrote the original draft. L.X., Y.P., Y.Q., Y.T.W., W.S. and Z.D. provided critical review. L.X. and Z.D. contributed to data presentation. L.X., Y.T.W., and Z.D. supervised the experiments. L.X., C.C., and Z.D. contributed to project administration. L.X., C.D., Y.D. and Z.D. obtained financial support. All authors contributed to the final manuscript. **Competing interests:** The authors declare that they have no competing interests. The Tat-BACE1$_{480-494}$ peptide in the manuscript has applied for the Chinese invention patent "BACE1 peptide and its application," which has not yet been granted and is the only patent related to this work. Z.D., L.X., J.L., and M.X. are all the authors. This patent was examined by the China National Intellectual Property Administration. The publication number of the invention patent application is CN118421606A. **Data and materials availability:** All data needed to evaluate the conclusions in the paper are present in the paper and/or the Supplementary Materials.

Submitted 11 October 2024
Accepted 18 April 2025
Published 23 May 2025
10.1126/sciadv.adt7981